



## Search for $WH$ Production using a Neural Network approach in $p\bar{p}$ Collisions at $\sqrt{s} = 1.96$ TeV with $1.7 \text{ fb}^{-1}$ of Data

(Dated: August 15, 2007)

A search for  $WH$  production in  $p\bar{p}$  collisions at a center of mass energy of  $\sqrt{s} = 1.96$  TeV is presented, combining the full Tevatron Run IIa dataset with the first part of the Run IIb dataset. The data correspond to an integrated luminosity of  $1.7 \text{ fb}^{-1}$  as accumulated by the DØ experiment. Events containing one lepton, missing transverse energy and one or two  $b$ -tagged jets are further selected using a neural network to enhance the potential  $WH$  signal over the standard model background. As no signal is observed, we set upper cross section limits between 1.06 and 1.42 pb at 95% C.L. (0.84 to 1.29 pb for the expected limits) on  $\sigma(p\bar{p} \rightarrow WH) \times B(H \rightarrow b\bar{b})$ , for Higgs masses between 105 and 145 GeV. For  $m_H = 115$  GeV, the observed (expected) limit is 1.42 (1.16) pb, to be compared to the expected standard model cross section of 0.13 pb.

*Preliminary Results for Summer 2007 Conferences*

## I. INTRODUCTION

For Higgs searches, the most sensitive production channel at the Tevatron for a Higgs mass ( $m_H$ ) below  $\sim 135$  GeV is the associated production of a Higgs boson with a  $W$  boson. The DØ collaboration has published a search for such production in the  $e\nu b\bar{b}$  decay channel using  $174 \text{ pb}^{-1}$  of integrated luminosity [1]. An update of that result using the  $e\nu b\bar{b}$  and  $\mu\nu b\bar{b}$  decay channels and a larger dataset of  $0.4 \text{ fb}^{-1}$  has been presented [2]. This has been further updated on  $\sim 1 \text{ fb}^{-1}$  of data using a cut-based approach and a matrix element discriminant approach. The result presented here, which uses more integrated luminosity, and a neural network approach to discriminate signal from background, supersedes our previous preliminary results. The CDF collaboration has published a  $WH$  production search on  $320 \text{ pb}^{-1}$  of data [3], and recently presented an update of the search with  $1 \text{ fb}^{-1}$  of data [4] using a neural network to reject background-like events having one jet identified as a  $b$ -jet.

Both  $e$  and  $\mu$  channels are also studied here. One lepton ( $e$  or  $\mu$ ), missing transverse energy  $\cancel{E}_T$  to account for the neutrino in the  $W$  boson decay and two or three jets are required, with at least one of them being  $b$ -tagged. Dominant backgrounds to the  $WH$  signal are  $W$ + heavy flavor production,  $t\bar{t}$  and single-top quark production. The channels are separated in events having exactly one “tight”  $b$ -tagged jet, and those having two “loose”  $b$ -tagged jet (with no overlap). We then apply a neural network (NN) discriminant to the selected events to separate the standard model background from the signal, and search for an excess at high values of the discriminant. The resulting four channels ( $e,\mu,1 \text{ } b\text{-tag}, 2 \text{ } b\text{-tag}$ ) are analyzed independently to optimize the sensitivity and then combined. In parallel, the four equivalent channels in  $W + 3$  jet events are also studied as a control sample.

The data set corresponds to an integrated luminosity of  $1.67 \text{ fb}^{-1}$  and consists of data recorded between April 2002 and February 2006 (Run IIa  $\sim 1.04 \text{ fb}^{-1}$ ) and data recorded between June 2006 and April 2007 (Run IIb  $\sim 0.63 \text{ fb}^{-1}$ ), i.e. after the Spring 06 Tevatron shutdown, during which the DØ detector was upgraded. In particular a new layer of silicon sensors of the microvertex detector was installed closer to the beam pipe, giving more precise track reconstruction. The two data periods are analyzed independently and then combined.

## II. DATA SAMPLE

The analysis relies on the following components of the DØ detector: a magnetic central-tracking system, which consists of a silicon microstrip tracker (SMT) and a central fiber tracker (CFT), both located within a 2 T superconducting solenoidal magnet [5]; a liquid-argon/uranium calorimeter made of a central section (CC) covering pseudorapidity  $|\eta|$  up to  $\approx 1.1$ , and two endcap calorimeters (EC) extending coverage to  $|\eta| < 4.0$ , all housed in separate cryostats [6], with scintillators between the CC and EC cryostats providing sampling of developing showers at  $1.1 < |\eta| < 1.4$ ; a muon system which resides beyond the calorimetry, and consists of a layer of tracking detectors and scintillation trigger counters before 1.8 T iron toroids.

The luminosity is measured using plastic scintillator arrays located in front of the EC cryostats, at  $2.7 < |\eta| < 4.4$ . The uncertainty on the measured luminosity is 6.1% [7]. We reject data periods in which the tracking (CFT and SMT), calorimeter or muon information may be compromised.

The trigger and data acquisition systems are designed to accommodate the large instantaneous luminosity of Run II. The events used in this analysis are triggered in the electron channel by a single trigger requiring an electromagnetic (EM) object and one jet (EM+jet). Triggers are taken into account in the simulation through event reweighting with an efficiency derived from data, and parametrized as a function of lepton azimuthal angle  $\varphi$  and  $\eta$ , and jet  $p_T$ . This efficiency is on average  $\sim 90\%$  for the events passing our requirements.

In the muon analysis we accept events from any trigger, since we expect close to 100% of our events to be triggered by our redundant triggering system (single muons, muon+jets, topological triggers). This is verified on RunIIa data using a combination of single-muon triggers for which a full analysis is completed. The efficiency of this trigger combination is measured on di-muon  $Z$  events with an uncertainty of 3%, and is  $\sim 70\%$  for the events passing our requirements, in the Run IIa sample. This efficiency is consistent with the overall increase in statistics (47% on average) that we observe in when accepting events from any trigger, both in data and in simulation, within  $\pm 3\%$  for the high statistics channels, and within  $\pm 10\%$  for the (low statistics)  $b$ -tagged channels. The shape of all distributions remains unchanged within the acceptance systematic uncertainty originating mainly from the jet energy scale uncertainty. We thus use all triggers for the final analysis, after attributing an additional 10% uncertainty on the trigger systematic in this channel. In Run IIb, we have used the same technique and verified that the events rates compared to the Run IIa rates are consistent within  $3\% \pm 9\%$  between the  $e$  channel (which uses dedicated triggers) and the  $\mu$  channel.

### III. SIMULATED DATASETS

Background and signal processes have been generated by different event generators as listed below. The PYTHIA [8] event generator, using the CTEQ6L1 [9] leading-order parton distribution functions, has been used to generate the following processes:

- Diboson processes:  $WW \rightarrow \ell\nu jj$ ;  $WZ \rightarrow \ell\nu jj$ ;  $WZ \rightarrow jj\ell\ell$ ; inclusive decays of  $ZZ$  ( $\ell = e$  or  $\mu$ )
- $WH \rightarrow \ell\nu b\bar{b}$  production ( $\ell = e, \mu, \text{ or } \tau$ )

The following processes are simulated using other generators:

- $W$ + jets and  $Z$ + jets events are generated with ALPGEN [10] (with PYTHIA radiation and showering), since ALPGEN yields a better description of processes with high jet multiplicity. ALPGEN samples have been produced using the MLM parton-jet matching prescription [10] and are generated in bins of light parton multiplicity.  $W(Z)$ + jets samples contain  $Wjj$  and  $Wcj$  processes, while  $Wb\bar{b}$  and  $Wc\bar{c}$  are generated separately.
- $Wb\bar{b}$  and  $Wc\bar{c}$  events are generated with ALPGEN requiring 2 heavy-flavored parton jets with  $p_T > 0$  GeV and  $|\eta| < 5.0$ , and “light parton” ( $u, d, s, \text{ and } g$ ) jets with  $p_T > 8$  GeV separated in  $\eta$ - $\varphi$  by  $\Delta R(\equiv \sqrt{\Delta\eta^2 + \Delta\varphi^2}) > 0.4$ . (for  $Wjj$  the partons cuts are  $p_T > 0$  GeV and  $\Delta R > 0.4$ ).
- $Zjj \rightarrow \ell lj j$ ,  $Zb\bar{b} \rightarrow \ell lb\bar{b}$  and  $Zc\bar{c} \rightarrow \ell lc\bar{c}$  ( $\ell = e, \mu \text{ or } \tau$ ) are generated with ALPGEN.
- $t\bar{t}$  (lepton+jet and dilepton channels) production is generated with ALPGEN.
- Single-top events ( $s$ -channel ( $tb$ ) and  $t$ -channel ( $tbq$ )) are generated using COMPHEP [11].

All the generated events were processed through the DØ detector simulation (based on GEANT [12]) and the reconstruction software.

The events used were simulated in the Run IIa detector configuration (i.e. without layer 0) since the difference between the Run IIa and Run IIb simulated events was observed to be small. They were then reweighted with Run IIa or Run IIb trigger efficiencies and efficiency ratios of data to simulation (scale factors), depending on the analyzed dataset. Depending on the efficiency considered these scale factors are constant or have a dependency on the event kinematics which is then taken into account, as discussed below.

The simulated background processes are absolutely normalized to the SM prediction of their cross section except  $W$ + jets which are normalized to data in the pre-tagged sample, where the signal contamination is expected to be negligible. The normalization factor data/MC  $\sim 0.97$  (0.85) in the  $W$  + 2 jet ( $W$  + 3 jet) sample, when we use the Next-to-Leading-Order (NLO) K-factor of 1.35 for the simulated  $Wjj$  sample, as determined using the program MCFM [13]. The normalization factor is derived after subtracting all other expected background processes from data, and is done independently in the 2 and 3 jet bin.

The K-factor used for  $Wb\bar{b}$  and for  $Wc\bar{c}$  has been empirically determined to be  $1.75 \pm 0.35$ , by adjusting the total number of background MC events to the data in the  $W$  + 2 jet sample, with at least one tight  $b$ -tagged jet. This is compatible with a MCFM calculation on  $Wbb$  using parton  $p_t > 8$  GeV, which gives 1.97. This computed K-factor was not used since our LO simulated sample use asymmetric cuts at the generator level: 8 GeV on light partons, 0 GeV on  $b$  and  $c$ -quarks. The same K-factors have been used for the corresponding  $Z$ + jet processes.

### IV. EVENT SELECTION

The analysis is based on the selection of events with exactly one electron (muon) with  $p_T > 15$  GeV and detector  $|\eta| < 1.1$  ( $< 2.0$ ), missing transverse energy  $\cancel{E}_T > 20$  GeV and two or three jets, with  $p_T > 20$  GeV (after jet energy scale corrections) and  $|\eta| < 2.5$ , with the further requirements that the leading jet has to have  $p_T > 25$  GeV, and that the sum ( $H_T$ ) of the  $p_T$  of the jets exceeds 60 GeV.

Events with an additional muon or electron, isolated from jets and having a transverse momentum above  $p_T > 20$  ( $> 15$  in the  $\mu$  channel) GeV are rejected to decrease the  $Z$  and  $t\bar{t}$  dilepton background. Only events having a primary  $z$ -vertex within  $\pm 60$  cm of the nominal interaction point and at least three attached tracks are retained for analysis.

### A. Lepton reconstruction and identification

The leptons used in the analysis are identified in two steps. 1) The lepton candidates are first required to pass the “loose” identification criteria, which for the electron are: energy fraction deposited in the EM calorimeter  $> 0.9$ , ratio of the energy in the hollow cone having external and internal radii of  $R = 0.4$  and  $0.2$  around the electron candidate direction, divided by the candidate energy  $< 0.15$ , shower shape requirements, and matching of an EM cluster to a track having  $p_T > 5$  GeV. For the muon, we require hits in each layer of the muon system, scintillator hits timing cuts to veto cosmics, matching between the muon track and a central track, and isolation from jets to reject muons from semi-leptonic hadron decays. 2) The loose leptons then undergo a final, “tight” selection: tight electrons have to satisfy a likelihood test developed on well-controlled samples, that takes as input seven quantities sensitive to the EM nature of the particles; tight muons must satisfy stricter isolation criteria requiring low calorimeter and tracking activity around the muon candidate. The inefficiencies induced by the lepton identification and isolation criteria are determined from dielectron and dimuon samples.

The final selection uses only tight leptons, whilst the sample of loose leptons is used for instrumental and semi-leptonic background determination

### B. Instrumental and semi-leptonic background

The instrumental and semi-leptonic backgrounds, so-called “QCD” background in the following, are estimated from the data. The instrumental background is important in the electron channel, where a jet with high EM fraction can pass the electron identification criteria. The semi-leptonic background is important in the muon channel, when the muon from a semi-leptonic heavy quark decay is mis-identified as being isolated.

To estimate the number of events containing a jet passing the final electron identification criteria we determine the probability  $p_{tight}^{loose}$  for a loose electron candidate originating from a jet to pass the likelihood test. This is done on data, using the sample of events used for the analysis after the preselection requirements, i.e. with one loose lepton and two jets, but with low  $\cancel{E}_T (< 10$  GeV), and in which one of the jets has an EM fraction smaller than  $0.7$ , is in the central calorimeter ( $|\eta| < 1.1$ ) and far from the calorimeter module boundaries. The probability  $p_{tight}^{loose}$  is obtained by dividing the number of events containing at least one electron candidate passing the likelihood test by the total number of events of the sample. This probability is determined as a function of the  $p_T$  of the candidate electron. We proceed similarly in the muon channel to determine the semi-leptonic background. We use the same selection criteria, but require a loose muon to be back-to-back in  $\varphi$  with one of the jets.

The QCD background is then estimated for every differential distribution: this  $p_T$ -dependent probability is used in the so-called matrix method that we apply to our final sample and to the loose sample. This method allows to derive the QCD background directly from data, once  $p_{tight}^{loose}$  and the lepton identification efficiency are known [14].

The  $p_T$  distribution of the lepton in the  $W + 2$  jet sample is shown in Fig.1a and compared to the expectation: at low  $p_T$  the contamination of QCD background is significant. The shape and magnitude of the distribution is well reproduced by the ALPGEN simulation of the  $W +$  jets processes, after adding the QCD background and other standard model (SM) backgrounds detailed in the previous section.

### C. Missing $E_T$ and Jet properties

To select  $W$  decays we require large missing transverse momentum,  $\cancel{E}_T > 20$  GeV.  $\cancel{E}_T$  is calculated from the calorimetric cells except unclustered cells in the coarse hadronic layers and is corrected for the presence of any muons. All energy corrections to muons or to jets are propagated into  $\cancel{E}_T$ .

The transverse mass  $m_T = \sqrt{2p_T^\ell p_T^\nu (1 - \cos(\varphi_\ell - \varphi_\nu))}$  of the  $W$  boson can be reconstructed from the charged lepton and neutrino ( $\nu$ ) kinematics quantities, in which the neutrino transverse momentum is approximated by the missing transverse energy. Its distribution is shown in Fig.1b. The distributions of  $H_T$  and missing transverse energy are shown in Fig.1c,d and compared to the expectation.

The jets used in this analysis are cone-type jets with a radius of  $R = 0.5$ . Identification requirements ensure that the jet energy distribution in the various layers of the calorimeter is reasonable and that the jets are not due to spurious energy deposits. The difference in efficiency of the jet identification requirement between data and simulation is taken into account in the overall jet reconstruction efficiency scale factor.

We have studied standard kinematic distributions and for example, the  $p_T$  distributions of the leading jet and next to leading jet in  $W + 2$  jet events are shown in Fig. 2a and b. The  $\eta$  distribution of the leading jet in the  $W + 2$  jet

	$W + 2$ jets	$W + 2$ jets (1 $b$ jet)	$W + 2$ jets (2 $b$ jets)	$W + 3$ jets	$W + 3$ jets (1 $b$ jet)	$W + 3$ jets (2 $b$ jets)
$WH$	$9.92 \pm 1.44$	$3.94 \pm 0.63$	$2.32 \pm 0.44$	$2.43 \pm 0.42$	$0.95 \pm 0.18$	$0.59 \pm 0.12$
$WZ$	$645 \pm 90$	$38 \pm 6$	$7.6 \pm 1.34$	$153 \pm 24$	$10 \pm 2$	$2.4 \pm 0.5$
$Wb\bar{b}$	$1352 \pm 346$	$441 \pm 117$	$91.7 \pm 26.0$	$433 \pm 118$	$137 \pm 39$	$33.9 \pm 10.0$
$t\bar{t}$	$348 \pm 83$	$139 \pm 34$	$53.8 \pm 14.3$	$596 \pm 152$	$238 \pm 63$	$122.4 \pm 34.3$
Single top	$189 \pm 37$	$78 \pm 16$	$19.4 \pm 4.4$	$62 \pm 13$	$25 \pm 6$	$10.1 \pm 2.5$
QCD Multijet	$2908 \pm 436$	$193 \pm 36$	$10.8 \pm 3.3$	$1051 \pm 158$	$87 \pm 16$	$12.2 \pm 4.7$
$W + \text{jets (light,c)}$	$28013 \pm 3181$	$470 \pm 137$	$20.9 \pm 6.9$	$5332 \pm 836$	$132 \pm 41$	$11.5 \pm 4.0$
Total expectation	33458 (n.t.d.)	$1360 \pm 187$	$204.1 \pm 31.0$	7627 (n.t.d.)	$630 \pm 86$	$192.5 \pm 36.3$
Observed Events	33458	1403	193	7627	570	173

TABLE I: Summary table for the  $W + 2,3$  jet final state. Observed events in data are compared to the expected number of  $W + 2$  jet events before tagging, after one tight  $b$ -tag, and after 2 loose  $b$ -tags. First (last) three columns,  $W + 2(3)$  jet channel. Expectation originates from the simulation of  $WH$  (with  $m_H = 115$  GeV), dibosons ( $WW, WZ, ZZ$ , labeled  $WZ$  in the table),  $Wb\bar{b}$  production, top production ( $t\bar{t}$  and single-top), QCD multijet background and “ $W + \text{jet}$ ” production, which contains light and  $c$  quarks. All  $Z$  processes are fully simulated, and included in the corresponding  $W$  categories. The processes  $W(Z)b\bar{b}$  and  $WH$  are counted separately. “n.t.d.” stands for “normalized to data”.

events is shown in Fig. 2c. The dijet invariant mass is shown in Fig. 2d. The shape of the distributions are described, within systematic errors, over the complete kinematic range for all jets.

## V. $b$ -TAGGING RESULTS

Since we search for  $WH$  production with two  $b$ -jets in the final state, efficient identification of  $b$ -jets in our selected events is a central part of the analysis. For tagging heavy flavored jets the  $D\emptyset$  neural network (NN)  $b$ -tagging algorithm has been used. It is based on the combination of seven  $b$ -hadron lifetime observables and all tagging and mistagging efficiencies have been determined on data and dedicated simulated samples.

We start with a “loose” NN operating point, which corresponds to a fake rate, i.e. the fraction of “light” partons ( $u, c, s, g$ ) mistakenly tagged as heavy-flavored jets by the tagger, of about 1.5% for a jet  $p_T$  of 50 GeV. If two jets are tagged the event is selected as double-tagged. Otherwise the operating point is tightened to a value corresponding to a fake rate of about 0.5%, and the event can then be selected as an “exclusive” single  $b$ -tag, simply called single  $b$ -tag in the following. We are thus left with two disjoint samples, one “loose” double-tag (DT) and one “tight” single-tag (ST) which simplifies their combination, done afterwards to improve the significance of a potential signal. The operating points have been selected based on the optimal combined sensitivity to a  $WH$  signal.

The efficiencies for identifying a jet containing a  $B$  hadron of the loose and tight operating points are about  $59 \pm 1\%$  and  $48 \pm 1\%$ , respectively, for a jet  $p_T$  of 50 GeV. The efficiency has been determined relative to taggable jets, i.e jets having at least 2 good quality tracks, of which one has  $p_T > 1$  GeV and another  $p_T > 0.5$  GeV. The jet taggability is typically 80% in a two jet QCD sample with an uncertainty of 3% per jet. The ratio between the expected taggability  $\times$  tagging efficiency in data vs. simulation is used to reweight (per jet) the simulated events in which one or more jet is tagged. The systematic uncertainty on this scale factor is 4-7% for heavy quarks ( $b, c$ ) and 25% when mis-tagging “light” partons.

The distributions of the  $p_T$  and  $\Delta R$  of the  $b$ -tagged jets for the  $W + 2b$ -jet events are shown in Fig. 3a and b. The observed agreement in both cases indicates that simulation, which includes the different standard model processes, describes the data well.

In total, we observe 1403 (570) single  $b$ -tagged events in the  $W + 2(3)$  jet channel, compared to  $1360 \pm 187$  ( $630 \pm 86$ ) expected events, as detailed in Table I. When requiring only one  $b$ -tagged jet, the background due to  $W + 2$  non- $b$  quark jets,  $t\bar{t}$  and QCD processes is a factor two larger than the contribution of the rare processes which can be studied with the upgraded Tevatron:  $Wb\bar{b}$ , single-top or Higgs production. To improve the signal to background ratio, we study single-tag and double-tag events separately.

In the  $W + 2(3)$  jet sample, the 193 (173) events observed in the DT channel are to be compared to an expected Standard Model background of  $204 \pm 31$  ( $193 \pm 36$ ) events, as detailed in Table I. In conclusion, the expectation describes the data well.

## VI. NEURAL NETWORK SELECTION

To optimize the sensitivity of the search, correlations between the kinematic properties of the objects in the event (lepton, jets,  $\cancel{E}_T$ ) are exploited using a neural network trained to separate Higgs signal events from background events. The neural network uses the following seven kinematic variables as inputs:

$$p_T(\text{leading jet}), p_T(2^{\text{nd}} \text{ jet}), \Delta R(\text{jets}), \Delta\phi(\text{jets}), p_T(\text{dijet system}), \text{dijet invariant mass}, p_T(\ell\text{-}\cancel{E}_T \text{ system})$$

For simplicity, the training of the neural network is performed using only simulated samples of Higgs and  $Wbb$  events in the muon channel, before application of any  $b$ -tagging requirements. Separate networks are trained and used for the different Higgs masses considered in the analysis.

Distributions of the neural network output trained on the  $m_H = 115$  GeV sample, after all selection cuts, are shown in Figs. 4a,b,c in the pre-tag, exclusive single-tag and double-tag samples. They are well described by the simulation. In Fig. 4d, the contribution of  $WH$  is shown to peak at high values of the neural network output, contrarily to the background. The neural network output is then fitted to separate the signal for the background as explained in section VIII. The same neural networks are used for the electron channel and the muon channel. The gain in sensitivity compared to the cut-based analysis (measured in terms of the final cross section limit) using this neural network approach is of the order of 10% depending on the Higgs mass, i.e. equivalent to a gain of about 20% in integrated luminosity.

## VII. SYSTEMATIC UNCERTAINTIES

The experimental systematic uncertainties due to efficiencies (i.e. the uncertainty on the ratio data/simulation of the efficiencies) or to the propagation of other systematic uncertainties (trigger, energy calibration, smearing), which affect the signal and standard model backgrounds (QCD background excepted) are summarized as follows:

- 3-10% uncertainty for the trigger efficiency derived from the data sample used in this analysis;  
5-6% uncertainty for the lepton identification and reconstruction efficiency.
- 2-6% uncertainty on the acceptance due to the jet identification and jet energy scale uncertainty.  
5% for the acceptance uncertainty due to jet modelling (fragmentation).
- 3% for the jet taggability, 2-5% for the  $b$ -tagging efficiency, per heavy quark jet. For the light quark jets the uncertainty is 25%; this translates into an uncertainty on the total background of the exclusive single-tag sample of 7% (negligible for double-tag)
- A shape uncertainty varying from -15% to +2% on the neural network output, originating from the modeling uncertainty of the  $W$ + jets background. This shape is obtained by comparing the original distribution to the one obtained after “reweighting” the selected events to a different set of ALGEN parameters, such that the expected dijet invariant mass distribution agrees with the data in the pre-tag sample, in which the signal is expected to be negligible.

Overall, the experimental systematic uncertainty on the acceptance varies between 16 and 30% depending on the process and the channel ( $\sim 18\%$  for  $WH$  in the DT channel).

The luminosity error is treated separately and amounts to 6%. The uncertainty on the cross sections of the background processes is 16% for  $t\bar{t}$  production and single-top production, 6% for  $WZ$  and  $WH$  production, and 20% for  $W$ + heavy flavor jets.

## VIII. $WH$ CROSS SECTION LIMIT

The expected contribution from the  $b\bar{b}$  decay of a standard model Higgs boson of 115 GeV, produced in association with a  $W$  boson is shown in Fig. 5a,b for the ST  $W+2,3$  jet channel, and in Fig. 5c,d for the DT  $W+2,3$  jet channels. It amounts to a total of 4.89 (2.91) events in the ST (DT) channels. As no excess is observed compared to the expectation, we proceed to set limits using the neural network output of the  $W + 2$  jet events. Each subchannel is analyzed independently. Limits are derived from the eight individual analyses ( $e, \mu$ , ST, DT) done with the  $W + 2$  jet events in the two different data taking periods (Run IIa and b), and then combined.

Limits are calculated at 95% confidence level using the modified Frequentist  $CL_s$  approach with a Poisson log-likelihood ratio test statistic [15, 16]. The impact of systematic uncertainties is incorporated through marginalization of the Poisson probability distributions for signal and background via Gaussian distribution. All correlations in systematic uncertainties are maintained amongst channels and between signal and background. The expected distributions for background are evaluated by minimizing a profile likelihood function, referencing the shape and rate of the observed distributions in the sideband regions.

The log-likelihood ratio (LLR) distributions for the  $WH \rightarrow \ell\nu b\bar{b}$ , (i.e. after combining the four individual  $W + 2$  jet subchannels) is shown in Fig. 6a. Included in the figure are the LLR values for the signal-plus-background hypothesis ( $LLR_{s+b}$ ), background-only hypothesis ( $LLR_b$ ), and the observed data ( $LLR_{obs}$ ). The shaded bands represent the 1 and 2 standard deviation departures for  $LLR_b$ . The cross section limit obtained for  $\sigma(p\bar{p} \rightarrow WH) \times B(H \rightarrow b\bar{b})$  is 0.59 pb at 95% C.L. for a Higgs boson mass of 115 GeV. The corresponding expected upper limit is 0.65 pb. The same study is performed for four other Higgs mass points: 105, 125, 135, and 145 GeV. The corresponding observed and expected limits are given in Table II. The ratio of these limits to the expected standard model values is shown in Fig. 6b. The limits obtained in this analysis are displayed in Fig. 7, where they are compared to the previously published results of DØ on 174 pb<sup>-1</sup> of data [1], CDF on 320 pb<sup>-1</sup> of data [3], and to the preliminary limits of CDF (1.7 fb<sup>-1</sup>) [4].

$m_H$ (GeV)	expected limit (pb)	observed limit (pb)
105	1.29	1.42
115	1.16	1.42
125	1.12	1.41
135	0.94	1.16
145	0.84	1.06

TABLE II: 95% C.L. expected and observed limits on  $\sigma(p\bar{p} \rightarrow WH) \times B(H \rightarrow b\bar{b})$  as a function of the Higgs mass.

The improvement in sensitivity obtained with the current analysis which combine extended acceptance/luminosity and multivariate technique is significant, in particular in the region where we have best sensitivity for low Higgs mass discovery, i.e. 115–135 GeV, with a ratio of observed (expected) limit to the SM cross section of  $\sim 9.1$  ( $\sim 11.1$ ) for  $m_H = 115$  GeV.

## IX. SUMMARY

The  $\ell + \cancel{E}_T + 2$  or 3 jets final state has been analyzed in the search for  $WH$  production in 1.7 fb<sup>-1</sup> of data taken between April 2002 and April 2007, split in two periods separated by the Spring '06 Tevatron shutdown. During the Tevatron shutdown DØ's triggering and  $b$ -tagging capabilities were upgraded.

We observe 193  $W + 2$  jet events with both jets  $b$ -tagged using a neural network  $b$ -tagging algorithm. The corresponding standard model expectation is  $204 \pm 31$  events. More generally, the production rate of these double  $b$ -tagged events is in agreement with the expected standard model cross sections, within statistical and systematic errors, both in  $W + 2$  and  $W + 3$  jet events.

The number of events with a  $W$  boson candidate and two jets in which one of the jets has been  $b$ -tagged with a tighter tagging operating point, and which does not belong to the double-tag sample is 1403 for an expectation of  $1360 \pm 187$  events. The single  $b$ -tagged production rate is consistent with the simulated expectation and the kinematic distributions of these events are also well described by the simulation.

The total expectation for Higgs production in this analysis amounts to 6.3 events, if  $m_H = 115$  GeV. To search for Higgs bosons of similar masses, we have combined all channels ( $e, \mu, ST, DT$ ) in  $W + 2$  jet events, and derived limits from the neural network discriminant distribution, using the  $CL_S$  method. We set upper cross section limits between 1.06 and 1.42 pb at 95% C.L. (0.84 to 1.29 pb for the expected limits) on  $\sigma(p\bar{p} \rightarrow WH) \times B(H \rightarrow b\bar{b})$  for Higgs masses between 105 and 145 GeV. For  $m_H = 115$  GeV, the observed (expected) limit is 1.42 (1.16) pb, to be compared to the standard model cross section expectation of 0.13 pb.

## Acknowledgments

We thank the staff at Fermilab and collaborating institutions, and acknowledge support from the Department of Energy and National Science Foundation (USA), Commissariat à l'Énergie Atomique and CNRS/Institut National de Physique Nucléaire et de Physique des Particules (France), Ministry for Science and Technology and Ministry for Atomic Energy (Russia), CAPES, CNPq and FAPERJ (Brazil), Departments of Atomic Energy and Science and Education (India), Colciencias (Colombia), CONACyT (Mexico), Ministry of Education and KOSEF (Korea), CONICET and UBACyT (Argentina), The Foundation for Fundamental Research on Matter (The Netherlands), PPARC (United Kingdom), Ministry of Education (Czech Republic), Natural Sciences and Engineering Research Council and West-Grid Project (Canada), BMBF (Germany), A.P. Sloan Foundation, Civilian Research and Development Foundation, Research Corporation, Texas Advanced Research Program, and the Alexander von Humboldt Foundation.

- 
- [1] DØ Collaboration, B. Abbott *et al.*, Phys. Rev. Lett. **94**, 091902 (2005)
  - [2] DØ Collaboration, B. Abbott *et al.*, *A search for WH Production at  $\sqrt{s} = 1.96$  TeV*, DØ Note 5054-CONF, <http://www-d0.fnal.gov/Run2Physics/WWW/results/prelim/HIGGS/H18/H18.pdf>
  - [3] CDF Collaboration, *Search for  $H \rightarrow b\bar{b}$  Produced in Association with W Bosons in  $p\bar{p}$  Collisions at  $\sqrt{s} = 1.96$  TeV*, hep-ex/0512051, Accepted in Phys. Rev. Lett.
  - [4] CDF Collaboration, CDF/ANAL/EXOTIC/PUBLIC/8957 (2007)
  - [5] DØ Collaboration, V. Abazov *et al.*, Nucl. Instrum. Meth., Res. A **565**, 463 (2006).
  - [6] S. Abachi, *et al.*, Nucl. Instrum. Methods Phys. Res. A **338**, 185 (1994).
  - [7] T. Andeen, *et al.*, “The DØ Experiment’s Integrated Luminosity for Tevatron Run IIa” FERMILAB-TM-2365, April 2007
  - [8] T. Sjostrand, P. Eden, C. Friberg, L. Lonnblad, G. Miu, S. Mrenna and E. Norrbin, “High-energy-physics event generation with PYTHIA,” Comput. Phys. Commun. **135**, (2001) 238, versions 6.319 and 6.323.
  - [9] H. L. Lai *et al.*, Improved Parton Distributions from Global Analysis of Recent Deep Inelastic Scattering and Inclusive Jet Data, Phys.Rev. D55 (1997) 1280, <http://hep.pa.msu.edu/people/wkt/cteq6/cteq6pdf.html>; J. Pumplin *et al.*, New Generation of Parton Distributions with Uncertainties from Global QCD Analysis, JHEP07(2002)012, arXiv:hep-ph/0201195v3.
  - [10] M. Mangano *et al.*: ALPGEN a generator for hard multiparton processes in hadron collisions, hep-ph/0206293, JHEP07 (2003) 001, version 2.05, <http://mlm.web.cern.ch/mlm/alpgen>.
  - [11] A. Pukhov *et al.*, COMPHEP, hep-ph/9908288 (1999)
  - [12] R. Brun and F. Carminati, CERN Program library Long Writeup, Report W5013 (1993).
  - [13] J. Campbell and K. Ellis, MCFM, Monte Carlo for FeMtobarn processes, <http://mcfm.fnal.gov/>
  - [14] S. Beauceron, Ph.D Thesis, University of Paris, 2004, [http://www-d0.fnal.gov/results/publications\\_talks/thesis/beauceron/thesis.pdf](http://www-d0.fnal.gov/results/publications_talks/thesis/beauceron/thesis.pdf).
  - [15] T. Junk, Nucl. Instrum. Meth. A434, p. 435-443, 1999.
  - [16] W. Fisher, DØ-Notes 4975 and 5309.

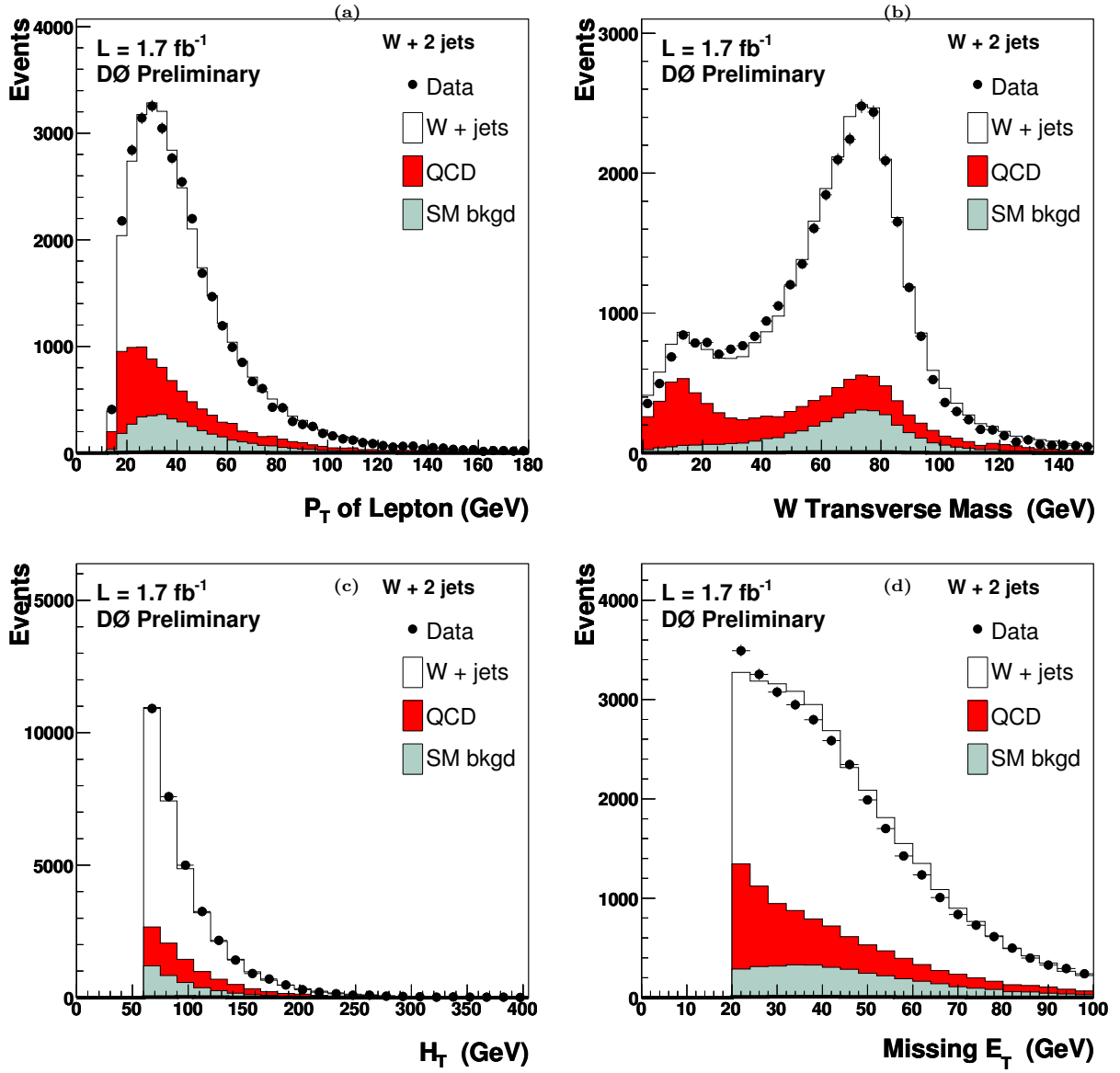


FIG. 1: Distributions of the lepton momentum (a), the transverse  $W$  mass (b), the  $H_T$  variable (c) and missing transverse energy (d) compared to the simulated expectation in the  $W + 2 \text{ jet}$  event sample. The simulation is normalized to the integrated luminosity of the data sample using the expected cross sections (absolute normalization) except for the  $W + \text{jets}$  sample which is normalized on the "untagged sample" to the data, taking into account all the other backgrounds.

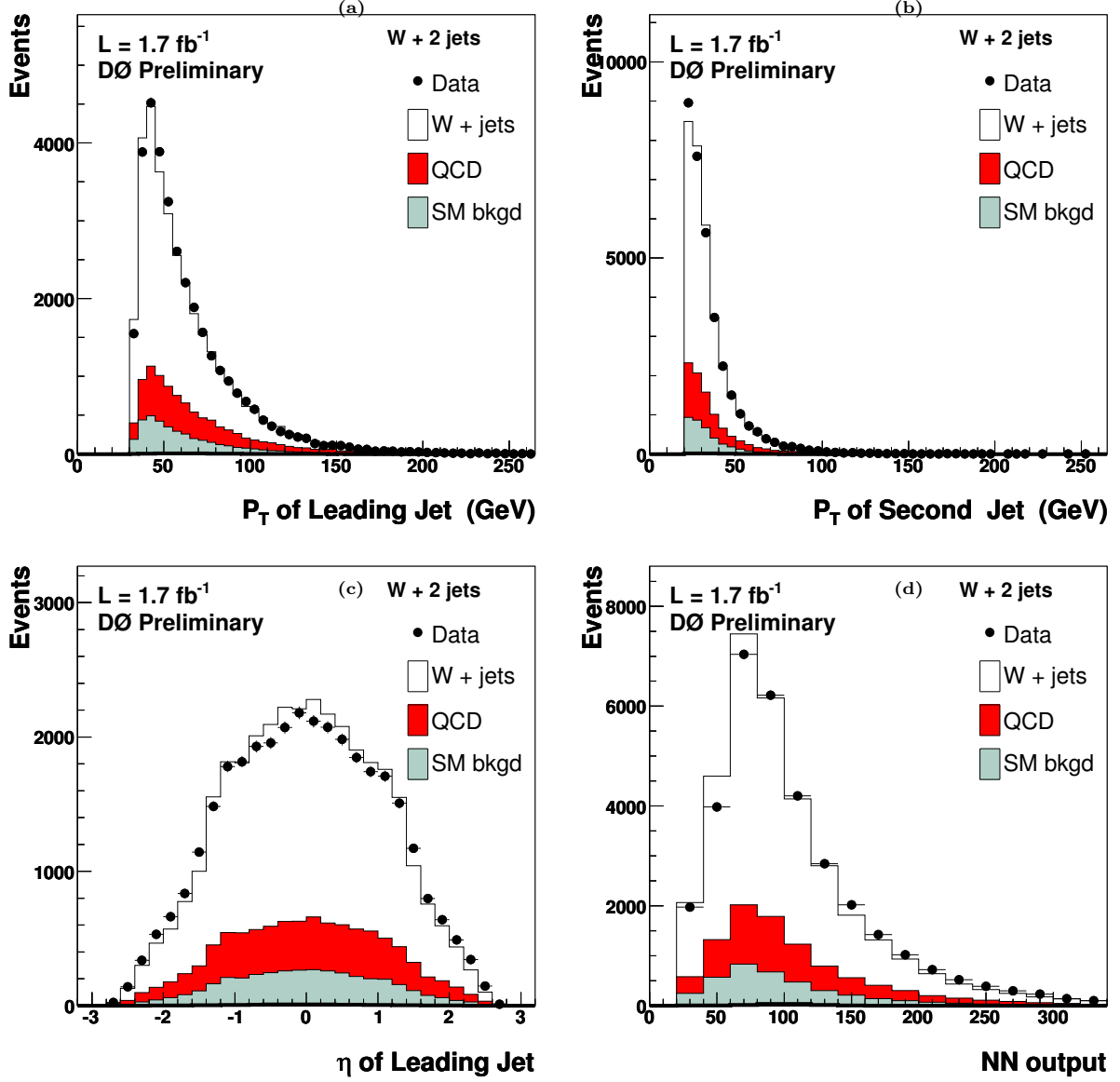


FIG. 2: Distribution of the  $p_T$  of the leading (a) and next to leading (b) jet, of the pseudorapidity of the leading jet (c) and of the dijet mass (d) between the two jets in the  $W + 2$  jet sample compared with the simulated expectation. The simulation is normalized to the integrated luminosity of the data sample using the expected cross sections (absolute normalization) except for the  $W + \text{jets}$  sample which is normalized on the "untagged sample" to the data, taking into account all the other backgrounds.

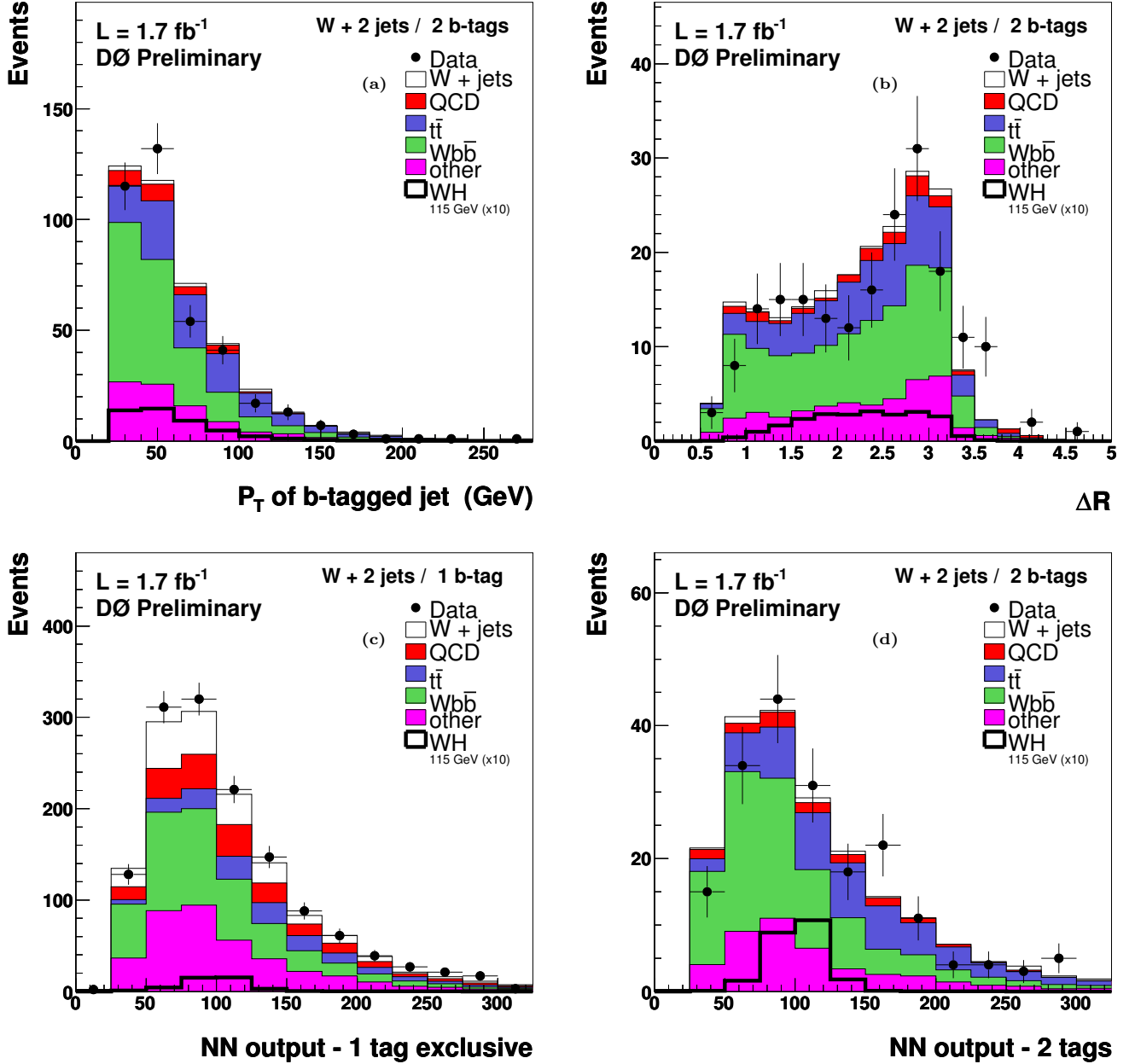


FIG. 3: (a,b): Distributions for the  $W + 2$  jet events having at least two jets b-tagged: a) b-tagged jets momentum; b)  $\Delta R$  between the two leading b-jets. c) (d) Dijet invariant mass in  $W + 2$  jet events having exactly one (two) jet b-tagged; The data are compared to the different simulated processes. The simulation is normalized to the integrated luminosity of the data sample using the expected cross sections (absolute normalization) except for the  $W + jets$  sample which is normalized on the "untagged sample" to the data, taking into account all the other backgrounds. Also shown is the contribution expected for standard model  $WH$  production with  $m_H = 115 \text{ GeV}$ , multiplied by a factor 10.

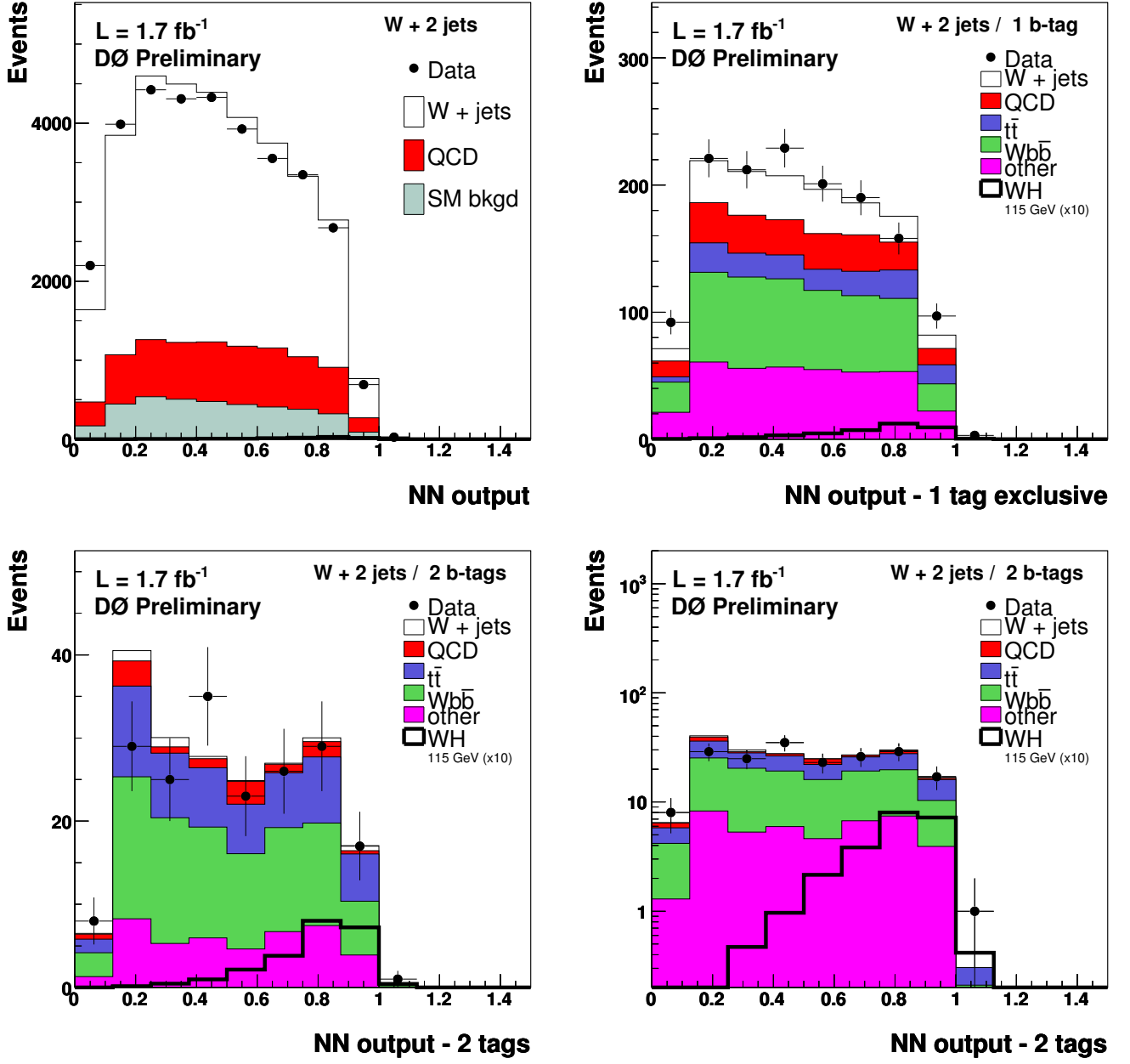


FIG. 4: Distributions of the neural network output compared with the simulated expectation: a) before b-tagging; b) in the exclusive single b-tag sample; c) in the double b-tag sample; d) same as c) with y logarithmic scale. The simulation is normalized to the integrated luminosity of the data sample using the expected cross sections (absolute normalization) except for the W + jets sample which is normalized on the "pre-tag sample" to the data, taking into account all the other backgrounds. The WH expected contribution is peaking at high values of the NN output as shown in d).

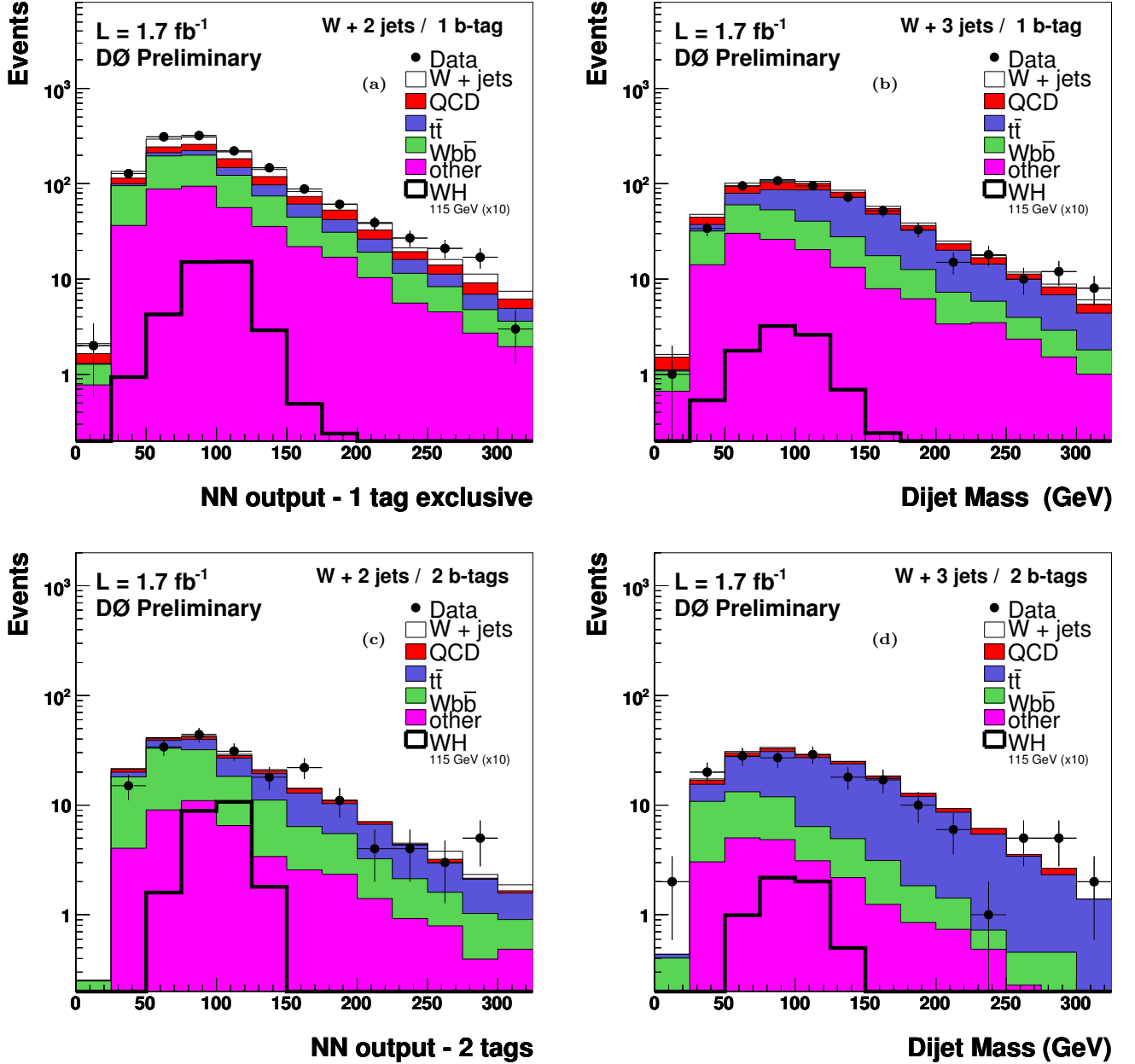


FIG. 5: a) (b) dijet invariant mass in  $W + 2(3)$  jet events when exactly one jet is b-tagged. c) (d) same distributions when at least 2 jets are b-tagged. The simulated processes are normalized to the integrated luminosity of the data sample using the expected cross sections (absolute normalization) except for the  $W +$  jets sample which is normalized on the "untagged sample" to the data, taking into account all the other backgrounds. The backgrounds labelled as "other" in the figure are dominated by single-top production. Also shown is the contribution expected for standard model  $WH$  production with  $m_H = 115$  GeV, multiplied by a factor 10.

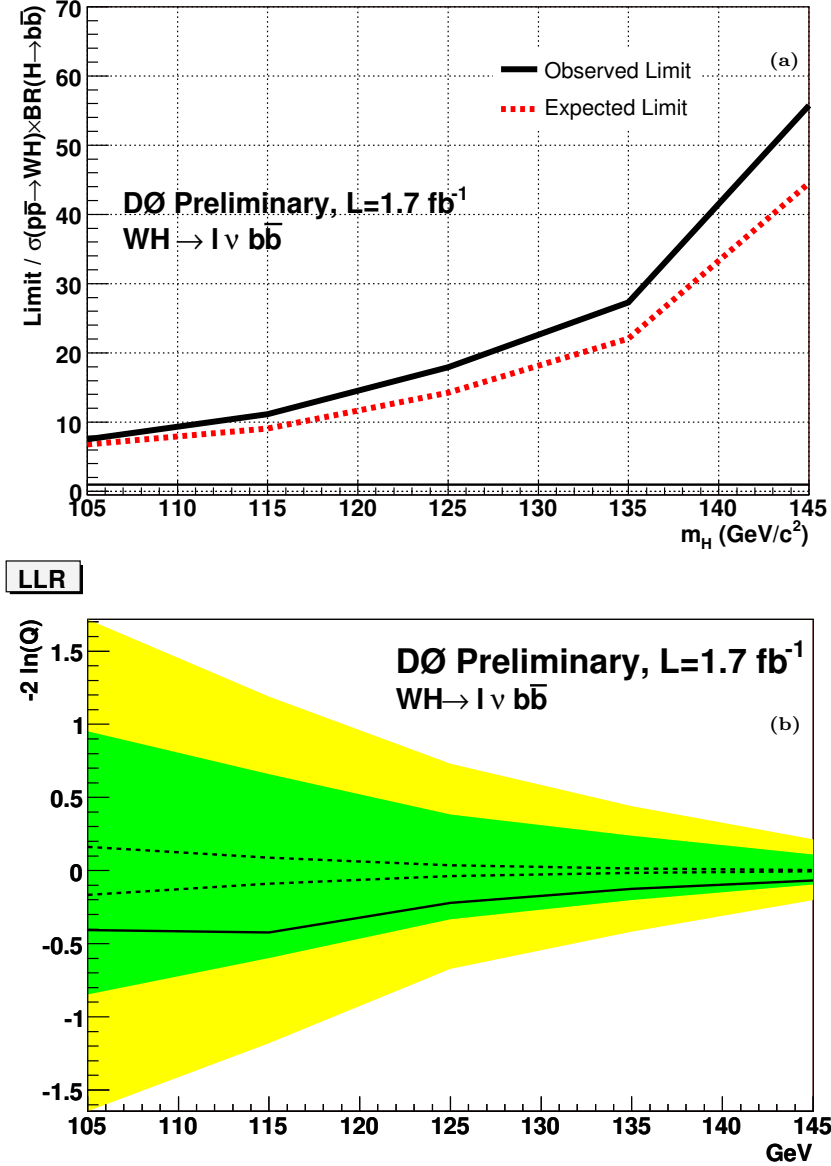


FIG. 6: Expected (median) and observed 95% C.L. upper limits on the cross section ratios in the neural network analysis for the combined  $WH \rightarrow e, \mu \nu b \bar{b} W + 2 \text{ jet}$  analyses (single- and double-tag, CC electrons + muons) in the  $m_H = 105 - 145$  GeV mass range. The solid line at  $y = 1$  indicates the 95% C.L. exclusion of the standard model expectation. b) Log-likelihood ratio distribution for the  $WH \rightarrow l \nu b \bar{b}$  2 jet channel. The dashed lines represent  $LLR_b$  (upper line)  $LLR_{s+b}$  (lower line), the full line represents  $LLR_{obs}$ ; for  $LLR_b$ , 1 and 2 standard deviation bands are drawn, cf section 8

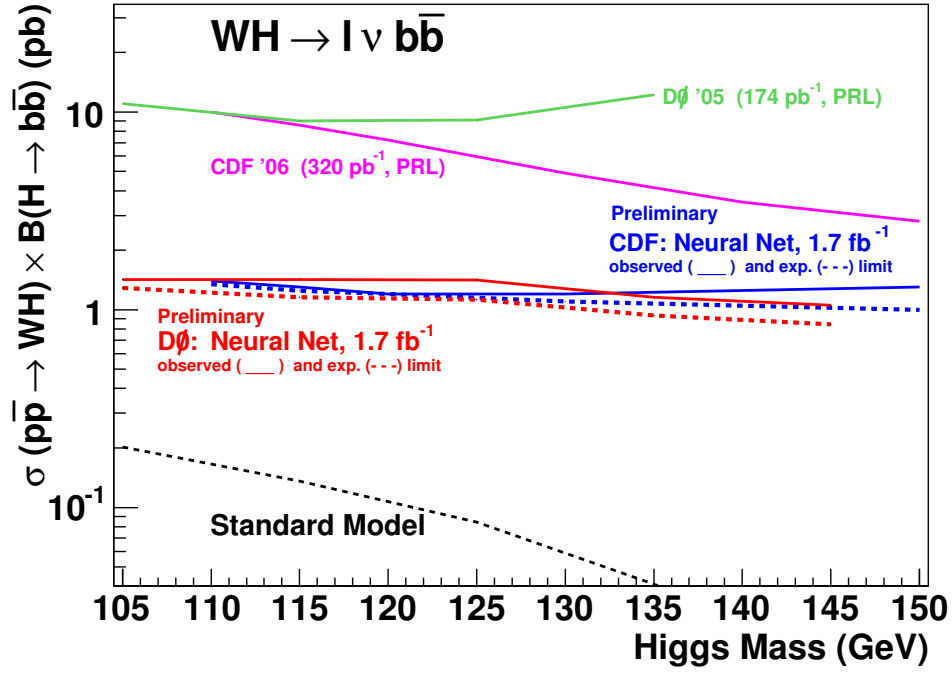


FIG. 7: 95% confidence level upper cross section limits on  $WH$  production derived after combining all  $W + 2$  jet channels ( $W$  boson decaying into a electron/muon + neutrino and Higgs into  $b\bar{b}$ ) vs. Higgs mass. This analysis is labeled “Neural Net” and is compared to an equivalent search by the CDF collaboration, to previous results, and to the Standard Model expectation, see text for details.